Journal of Materials Research and Technology 42 (2026) 1352–1356

Contents lists available at ScienceDirect

Journal of Materials Research and Technology

journal homepage: www.elsevier.com/locate/jmrt

Soft-mechanochemical synthesis of Fe–B amorphous nanoparticles for the preparation of Fe–B nanoglass

Chaomin Wang [a,b,*], Peng Chen [b,c], Chunyu Guo [d], Qi Liu [c,e], Huihui Yu [a,b], Yulia Ivanisenko [f,**]

[a] Jiangxi Key Laboratory of Advanced Copper-based Materials, 330012, Nanchang, China
[b] Institute of Materials and Intelligent Manufacturing, Jiangxi Academy of Sciences, 330012, Nanchang, China
[c] Institute of Energy Research, Jiangxi Academy of Sciences, 330012, Nanchang, China
[d] School of Mechanical Engineering, Changzhou Institute of Technology, 213163, Changzhou, China
[e] Jiangxi Provincial Key Laboratory of Greenhouse Gas Accounting and Carbon Reduction, 330012, Nanchang, China
[f] Institute of Nanotechnology, Karlsruhe Institute of Technology, Eggenstein-Leopoldshafen, 76344, Germany

ARTICLE INFO

Keywords:
Amorphous
Nanoparticles
Nanoglass
Soft-mechanochemical
Nanoindentation

ABSTRACT

Synthesis of high-purity and ultrafine amorphous nanoparticles (AmN) is critical for nanoglass fabrication. Herein, high-purity $Fe_{67}B_{33}$ AmN with an average particle size of ~12.5 nm were synthesized for the first time via a soft-mechanochemical method. These AmN were consolidated into a partially dense Fe–B nanoglass with a crystallization temperature of ~450 °C. Nanoindentation tests reveal that the nanoglass has an average hardness of 6.6 ± 0.3 GPa and an elastic modulus of 114 ± 4 GPa, and undergoes homogeneous deformation without shear band formation. This work demonstrates the soft-mechanochemical method as a promising route for preparing ultrafine AmN for nanoglass fabrication.

1. Introduction

Nanoglass is a novel type of bulk non-crystalline materials composed of nanoscale non-crystalline cores and low-density interfaces, in which the interfaces contain more free volume than the cores and the traditional non-crystalline materials [1,2]. Due to such a unique nanostructure, nanoglasses exhibit many properties different from those of the traditional non-crystalline materials with similar chemical compositions [1–8]. For instance, $Fe_{90}Sc_{10}$ nanoglass prepared by consolidating $Fe_{90}Sc_{10}$ glassy nanoparticles is ferromagnetic at room temperature, while $Fe_{90}Sc_{10}$ melt-spun ribbons are paramagnetic [3].

Nowadays, the main approach to prepare a nanoglass is to prepare high-purity and ultrafine glassy or amorphous nanoparticles (AmN) first, and then consolidate these nanoparticles into a non-crystalline bulk block [1,2]. High purity of AmN is a prerequisite for obtaining high-purity nanoglass, while the small particle size is beneficial for the preparation and performance improvement of nanoglass [8,9]. For example, for some metallic nanoparticles with an average particle size of 50 nm, if we assume the thickness of the interfaces within nanoglass as 2 nm, the corresponding volume fraction of the interfaces may be smaller than 12% according to the estimation [8,10]. For the 12.5 nm Fe–B AmN synthesized in this work, the interface volume fraction is calculated to be ~48% based on the same interface thickness assumption, which is much higher than that of 50 nm nanoparticles. Thus, as the particle size of AmN increases, the volume fraction of the interfaces decreases, leading to inferior properties of nanoglasses [8,9]. Additionally, it is harder to consolidate the larger amorphous particles into dense bulk amorphous materials. For instance, Wang et al. consolidated submicron-sized Fe–B amorphous particles with average particle sizes of 116 to 576 nm at 300 K for 1 h, but the obtained samples were partially crystallized and contained big pores inside [11].

Until now, the inert gas condensation (IGC) seems the best approach to prepare high-purity and ultrafine non-crystalline nanoparticles [1–8,10]. However, few research groups have been able to prepare nanoglasses via this route, probably because the IGC equipment is too expensive and inefficient. Moreover, the IGC method features extremely poor scalability, hindering large-scale industrial production, and its compositional tunability is low because the vapor pressure differences between different elements lead to inaccurate compositional control. Chemical methods can be applied for any research group, however, it is hard to synthesize AmN and most of the synthesized AmN were neither clean nor small enough [12–14]. This may be because the AmN are in a

* Corresponding author. Jiangxi Key Laboratory of Advanced Copper-based Materials, 330012, Nanchang, China.
** Corresponding author.
E-mail addresses: wangchaomin@jxas.ac.cn (C. Wang), julia.ivanisenko@kit.edu (Y. Ivanisenko).

https://doi.org/10.1016/j.jmrt.2026.03.167
Received 26 December 2025; Received in revised form 2 March 2026; Accepted 18 March 2026
Available online 19 March 2026

metastable state with higher energy than the crystalline nanoparticles, and their surface energy will further increase with the decrease of their particle sizes [15]. Therefore, the adhesive force between nanoparticles increases, leading to severe aggregation of small nanoparticles and the formation of large particles [16]. For instance, the average particle size of Fe–B AmN synthesized by liquid-state chemical reduction without using surfactants was generally larger than 50 nm [17–21], and these particles suffer from severe aggregation, which limits their application in nanoglass preparation. Although some ultrafine AmN could be synthesized by absorbing surfactants to decrease their surface energy [12–14,16], these AmN also could not be used for preparation of nanoglasses since their surfaces were not clean.

Nowadays, the soft-mechanochemical method is used to prepare AmN without any surfactants [22–25], which indicates its potential for synthesizing high-purity AmN for nanoglass preparation. Fe–B AmN have been intensively studied due to their wide applications in catalysis, magnetorheological fluids, magnetic devices, anodes et al. [12,13,17–21,26]. Since Fe–B AmN have been synthesized via several other methods [12,13,17–21,26] except the soft-mechanochemical approach, these methods for Fe–B AmN have the defects of large particle size and severe aggregation, forming a scientific gap in the preparation of high-purity and ultrafine Fe–B AmN. Herein, we attempted to synthesize Fe–B AmN to prove the potential of the soft-mechanochemical method and further improve the properties of Fe–B AmN. This method is applied for the first time to successfully synthesize high-purity Fe–B AmN with an average particle size of ~12.5 nm. It breaks through the limitations of traditional liquid-phase reduction and mechanical alloying in the preparation of Fe–B AmN (large particle size, easy aggregation, high impurity content), and provides a new approach for preparing high-purity and ultrafine AmN for the preparation of nanoglasses.

2. Methods

Powders of $NaBH_4$ (98 wt%), $FeCl_2$ (anhydrous, 99.5 wt%) and NaCl (99.99 wt%), purchased from Shanghai Aladdin Reagent Co. Ltd, were used for the soft-mechanochemical synthesis without any purification. The whole process of powder preparation was carried out under oxygen-free conditions. First, in a Mikrouna glove-box filled with high-purity argon (5 N), the raw materials (3.8025 g $FeCl_2$, 2.2700 g $NaBH_4$ and 0.6000 g NaCl) were put into a 250 mL agate jar. The agate milling balls with a diameter of 10 mm were then added into the jar, and the weight ratio of milling balls to materials was about 15:1 (an appropriate ratio for soft-mechanochemical synthesis, ensuring sufficient grinding and mixing without excessive particle collision). The jar was then tightly sealed with an O-ring. In this process, both O_2 and H_2O content in the glove-box were kept below 1 ppm. The sealed jars were then loaded in the planetary ball mill (QM-3SP2 mill from Nanjing University Instrument Company, the ratio of rotation speed to revolution speed is −2:1) for ball milling. The rotation speed was set at 160 rpm (a low speed determined by pre-experiments to avoid particle aggregation and crystallization), and the milling was stopped for 10 min every 20 min (intermittent pause avoids excessive system temperature rise). The total milling time was 9 h (pre-experiment verified that this time is sufficient for complete solid-state reaction, further milling may cause crystallization). After the ball milling, the jars were opened in the glove box to collect the gray powder. The powder was washed (in the glove box) with deionized water for 4 times, and then washed with acetone and deionized water for another 6 times alternately, and the last time was washed with acetone. Prior to this, the deionized water and acetone were bubbled with high-purity argon (5 N) for several hours to remove the dissolved oxygen. Subsequently, the washed powder was dried in the vacuum oven (in the glove box) at 60 °C for 12 h to obtain the dry Fe–B powder. The final yield of Fe–B AmN after washing and drying is ~75%. The mass loss is mainly attributed to the dissolution of a small amount of unreacted raw materials and incomplete centrifugation.

In the glove box, 0.15 g Fe–B powder was consolidated in the powder-consolidation mold to obtain a metallic pellet. The consolidation pressure was increased very slowly, and was held for 2 min at 1 GPa and 2 GPa, respectively. Finally, the consolidation pressure was held for 3 min at 3 GPa and then was released slowly to zero to obtain a metallic pellet with a diameter of 10 mm and thickness of ~0.4 mm. The stepwise pressure increase mode reduces interparticle porosity and prevents crystallization of AmN induced by one-step high pressure. The holding time is determined by pre-experiments to ensure uniform pressure transfer and avoid crystallization.

The amorphous structure of the powder was characterized by X-ray diffraction (XRD). The dried powder was sealed with Kapton tape in the glove box to prevent it from contacting the air. Then the sealed powder was taken out of the glove box for the XRD measurement. At the same time, in order to distinguish the influence of Kapton tape, the blank Kapton tape was measured in the same way for comparison. The metallic pellet was taken out of the glove box directly for testing. The XRD measurement was carried out using the Bruker D8 Advance X-ray diffractometer equipped with a cobalt target source. The data acquisition range was 20-80°, the scanning rate was $4^\circ \cdot min^{-1}$, and the scanning step was 0.02°. The sample for transmission electron microscopy (TEM) was also prepared in the glove box. After cleaning as described above, a small amount of wet powder was dispersed with acetone to make a suspension, which was dropped onto a copper grid loaded with carbon film. The TEM characterization was carried out on a Talos F200X electron microscope with an accelerating voltage of 200 kV. The particle size statistics of Fe–B AmN were completed by counting 240 nanoparticles from the TEM images via ImageJ software. The composition identification of AmN was characterized using an Agilent 5110 inductively coupled plasma optical emission spectrometry (ICP-OES). The absolute detection limits of this ICP-OES for Fe, B, Si, and Na are 0.02, 0.40, 0.10, and 0.12 ppm, respectively. The digestion step for ICP-OES test is as follows: ~10 mg of the sample was accurately weighed using an analytical balance, then wetted with a small amount of deionized water, followed by the addition of 10 mL of aqua regia as the digestion reagent. The digestion tank was tightly sealed and placed into the microwave digester with a protective outer tank. A pre-digestion step was first performed at 120 °C for 30 min, and then the multi-step microwave digestion program was initiated. First, the temperature was raised to 130 °C over 5 min and held for 3 min, subsequently it was raised to 150 °C over 3 min and held for 10 min, and finally it was raised to 180 °C over 3 min and held for 30 min. After the digestion program was completed, the tank was naturally cooled down to 60 °C, and the resulting digest solution was transferred to a volumetric flask and diluted to the 25 mL mark with deionized water for subsequent ICP-OES testing.

Differential scanning calorimetry (DSC) measurement of nanoglass was carried out on a NETZSCH DSC 404F3, and the samples were heated from 50 °C to 800 °C at a rate of 10 $°C \cdot min^{-1}$. The mechanical test of nanoglass was carried out in the continuous stiffness mode on the Bruker Hysitron TI980 nanoindentation tester. The maximum load was 10 mN, and the loading rate was 0.1 s^{-1}. The vibration frequency was 220 Hz. The load was maintained for 2 s, the unloading time was 5 s, and the drift control target value was 0.05 nm s^{-1}. The maximum indentation depth in the nanoindentation tests was ~300 nm, and the ratio of indentation depth to sample thickness is far less than 1%, which effectively eliminates the substrate effect. Prior to the nanoindentation tests, the surface of nanoglass sample was polished to a mirror surface with oxide polishing suspension. Nanoindentation tests were performed at 8 different points on the sample surface, and the distance between adjacent points was more than 10 μm. Scanning electron microscopy (SEM) images of the indented areas were obtained using a Zeiss Gemini 300 scanning electron microscope, and the SEM sample was sputtered with gold nanoparticles to enhance conductivity.

3. Results and discussion

Figure 1 shows the XRD patterns of the blank Kapton tape (black curve) and the sealed Kapton tape with the Fe–B powder inside (red curve). Comparing these two patterns, it can be seen that there are no other diffraction peaks of the Fe–B powder except the main broad peak at ~52.5° representing the amorphous structure.

Figure 2 shows the -TEM characterization results of the Fe–B powders. From the TEM image in Fig. 2a, it can be seen that the as-prepared powder is composed of nanoparticles, and the nanoparticles have near spherical shape. These nanoparticles exhibit no obvious aggregation, which is favorable for the subsequent consolidation of nanoglass. The electron diffraction pattern of these nanoparticles in the inset of Fig. 2a shows uniform diffraction rings without any diffraction spots, which proves that the as-prepared powder is amorphous. This is consistent with the high-resolution TEM image as shown in Fig. 2b, which further proves that these nanoparticles are fully amorphous without any lattice. The average particle size (D_{TEM}) was counted as ~12.5 nm, and the particle size is mainly distributed in 8~16 nm as shown in the particle size distribution histogram in Fig. 2c.

The composition of Fe–B powder was quantitatively analyzed by ICP-OES. Silicon, as the main component of agate milling balls and jars, was not detected. This can be mainly attributed to the gentleness of the milling. Since $NaBH_4$ could easily reduce $FeCl_2$ [17–21], ball milling was only used to help refine and to mix the materials to trigger the solid-state reaction. In addition, agate milling balls have a low density (~2.6 $g{\cdot}cm^{-3}$), and the mill was operated at a very low rotation speed for a relatively short time, resulting in low impact and shear forces exerted by the balls. Thus, this gentle approach can be called the Soft-mechanochemical Method [24]. Meanwhile, the method of milling pure iron and boron powders to form alloyed Fe–B amorphous powder was called the Mechanical Alloying Method [27,28]. This method requires high-energy ball milling with heavy milling balls (normally steel with a density of ~7.9 $g{\cdot}cm^{-3}$) at a much higher mill rotation speed or ball-to-powder ratio to generate large impact and shear forces for alloying the metals. This process typically takes more than 200 h and thus introduces considerable impurities from the milling balls and jars [27,28]. Furthermore, only micron-sized Fe–B amorphous particles can be prepared [27,28]. In this work, the agate milling balls and jars were not worn during a short time of gentle milling, so additional impurities could be avoided. In addition, no Na could be detected, indicating that the content of Na impurity in the Fe–B AmN is below 0.12 ppm, which fully proves the high purity of the prepared powder. Therefore, it can be considered that high-purity AmN with an average composition of about Fe_2B ($Fe_{67}B_{33}$) has been successfully synthesized.

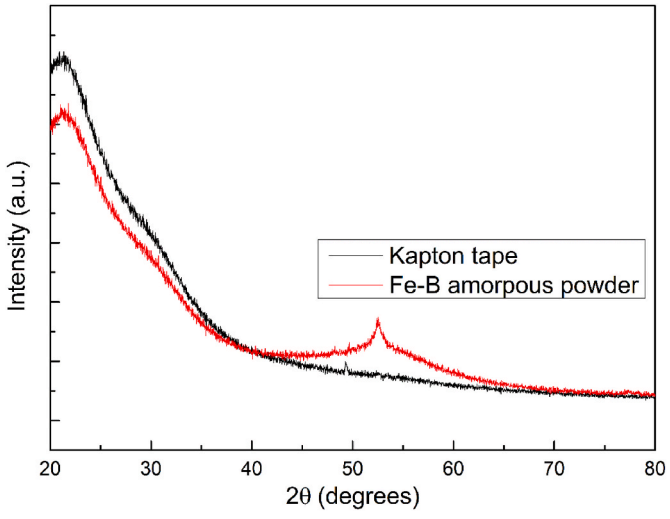

Fig. 1. The XRD patterns of the blank Kapton tape (black curve) and the sealed Kapton tape with Fe–B powder inside (red curve).

From the above results, it can be seen that the soft-mechanochemical method could be used to successfully synthesize Fe–B AmN which are finer and better dispersed in comparison with powders prepared by liquid-state reaction [17–21]. Since most chemical synthesis (in liquid phase) can be replaced by soft-mechanochemical synthesis [23,24], the AmN prepared in liquid phase can also be prepared by mechanochemical method [22,25]. In other words, the soft-mechanochemical route has the potential to become a new approach for synthesizing many other high-purity and ultrafine AmN.

Based on the molar ratio of $FeCl_2$ to $NaBH_4$ and the ratio of iron to boron atoms in the products, it is hypothesized that the solid-state reaction in the present work may be expressed as [17]:

$$NaBH_4 + 2FeCl_2 = Fe_2B + 3HCl + NaCl + 0.5H_2\uparrow \quad (1)$$

Both the NaCl generated in reaction (1) and the added NaCl act as a diluent [25]. Since reaction (1) can release a large amount of heat, NaCl dispersed between reactants can absorb heat to lower the temperature of the system, thus significantly reducing the reaction rate [25]. Because the reaction (1) is much slower than that of the liquid-state reaction, the generated nanoparticles are much smaller than those generated in the latter case. At the same time, NaCl could also act as an absorbent on the surfaces of Fe–B AmN to decrease their surface energy, and also could act as a barrier between Fe–B AmN to decrease their aggregation [16]. Consequently, the AmN were further refined with improved dispersion.

Figure 3a is the XRD pattern of the metallic pellet (as shown in the inset of Fig. 3a) obtained by consolidation of Fe–B AmN. The broad peak indicates the amorphous structure of the sample. The DSC curve in Fig. 3b shows that the metallic pellet has an obvious crystallization peak, and the crystallization temperature is ~450 °C. This crystallization temperature is close to that of mechanically alloyed $Fe_{70}B_{30}$ amorphous alloys (crystallization temperature is ~465 °C, measured by DSC at a heating rate of 20 $°C{\cdot}min^{-1}$) with a similar composition [27]. Therefore, it can be concluded that the nanoglass has been successfully prepared by consolidation of Fe–B AmN.

Figure 4a shows the nanoindentation load versus displacement curves obtained at eight different points of the pellet. Fig. 4b and c shows the hardness and modulus versus the displacement curves, respectively. From these results, it can be seen that there was little scatter between the results of eight tests, which proved that the results were reliable. The average hardness and elastic modulus of the sample are ~6.6 ± 0.3 GPa and ~114 ± 4 GPa, respectively. In addition to the statistical measurement error, the difference between the results might be caused by the tiny density fluctuation of the nanoglass sample. The density fluctuation may be due to incomplete consolidation of the powder. The morphology of the indent of the surface of the nanoglass sample was observed by scanning electron microscope, and no shear bands appeared around the indentation (Fig. 4d). This is consistent with the curves in Fig. 4a that the load-displacement curves are smooth without any pop-ins, which indicates that the nanoglass underwent homogeneous deformation [6,7]. This is mainly because nanoglass contains a large number of low-density interfaces with high free volume. These low-density interfaces provide a large number of nucleation sites for the shear transformation zones (STZ), which makes the STZ uniformly nucleate and evolve during the deformation process, thus realizing homogeneous deformation without shear band formation [6,7].

4. Conclusions

High-purity, ultrafine $Fe_{67}B_{33}$ AmN (average particle size of ~12.5 nm) have been prepared via a soft-mechanochemical approach. Partially dense $Fe_{67}B_{33}$ nanoglass was then prepared by consolidation of these AmN. The crystallization temperature of the nanoglass is ~450 °C. The average hardness and elastic modulus are ~6.6 ± 0.3 GPa and ~114 ± 4 GPa, respectively. This nanoglass exhibits notably homogeneous

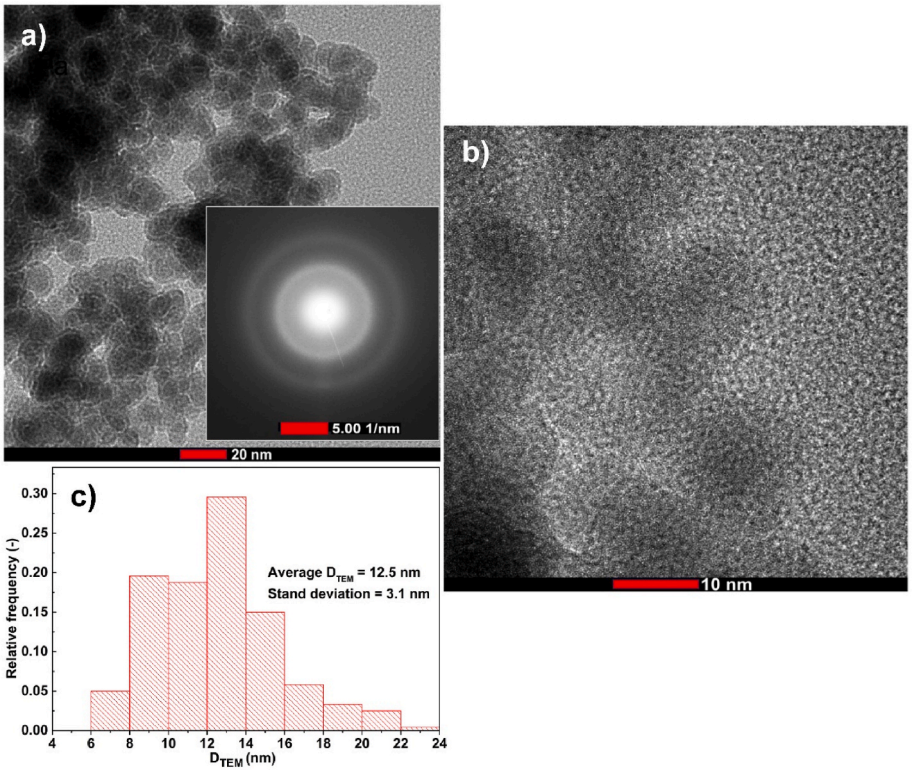

Fig. 2. TEM characterization results of the Fe–B powders. (a) TEM image with the corresponding electron diffraction pattern shown in the inset; (b) High-resolution TEM image; (c) Particle size distribution estimated from TEM images.

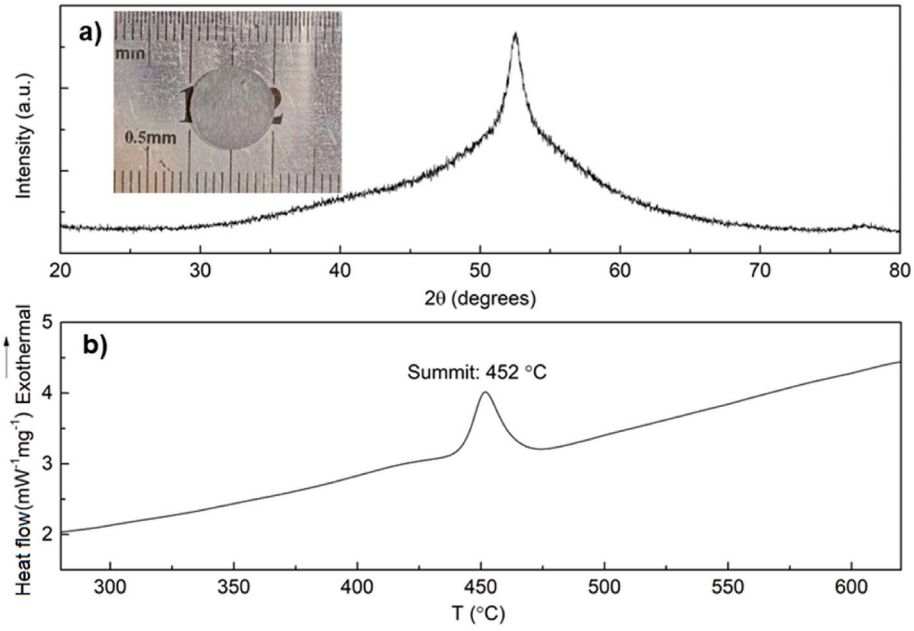

Fig. 3. The XRD pattern (a) and the DSC curve (b) of the Fe–B nanoglass. The inset of (a) shows the photo of the Fe–B nanoglass pellet placed on a ruler.

deformation without the formation of shear bands during nano-indentation. In the future, the consolidation process will be further optimized to improve the densification of Fe–B nanoglass, and long-term thermal stability and other functional property tests will be conducted to expand the application of Fe–B nanoglass in practical engineering.

Declaration of competing interest

The authors declare the following financial interests/personal relationships which may be considered as potential competing interests: Chaomin Wang and Yulia Ivanisenko reports financial support was provided by Jiangxi Provincial Department of Science and Technology. Chaomin Wang, Peng Chen, Qi Liu, Huihui Yu reports equipment, drugs, or supplies was provided by Jiangxi Key Laboratory of Advanced

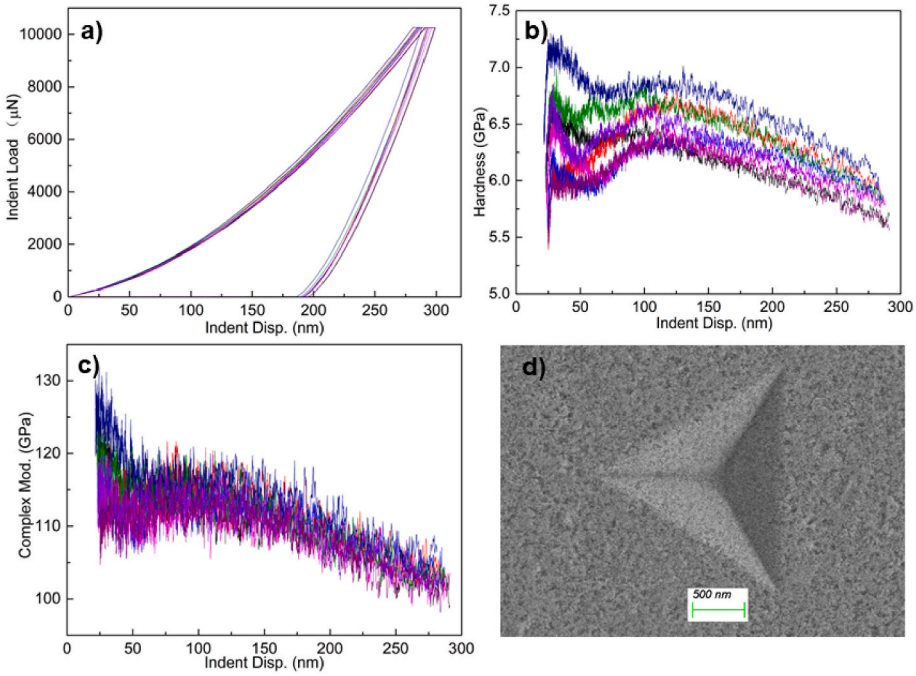

Fig. 4. The characterization results of the Fe–B nanoglass from nanoindentation experiments at eight distinct points. (a) Load versus displacement curves; (b) Hardness versus indentation depth curves; (c) Elastic modulus versus indentation depth curves; (d) A representative SEM image of a nanoindent.

Copper-based Materials. If there are other authors, they declare that they have no known competing financial interests or personal relationships that could have appeared to influence the work reported in this paper.

Acknowledgements

This work was supported by Jiangxi Provincial Department of Science and Technology (grant number 20203BDH80W008) and Jiangxi Key Laboratory of Advanced Copper-based Materials (grant number 2024SSY05021).

References

[1] Gleiter H, Schimmel T, Hahn H. Nanostructured solids – from nanoglasses to quantum transistors. Nano Today 2014;9:17–68.
[2] Ivanisenko Y, Kübel C, Nandam SH, Wang C, Mu X, Adjaoud O, et al. Structure and properties of nanoglasses. Adv Eng Mater 2018;20:1800404.
[3] Witte R, Feng T, Fang J, Fischer A, Ghafari M, Kruk R, et al. Evidence for enhanced ferromagnetism in an iron-based nanoglass. Appl Phys Lett 2013;103:073106.
[4] Wang C, Palit M, Yin N, Shi Q, Ivanisenko Y, Gleiter H, et al. Magnetic contributions to the low-temperature specific heat of $Sc_{79}Fe_{21}$ nanoglass. J Appl Phys 2019;125:045111.
[5] Wang C, Hu Q, Luo J, Yin N, Shi Q, Gleiter H, et al. Enhanced specific heat of the $Sc_{79}Fe_{21}$ nanoglass compared to the $Sc_{79}Fe_{21}$ amorphous melt-spun ribbon in a temperature range of 150–300 K. Mater Lett 2023;349:134706.
[6] Nandam SH, Ivanisenko Y, Schwaiger R, Śniadecki Z, Mu X, Wang D, et al. Cu-Zr nanoglasses: atomic structure, thermal stability and indentation properties. Acta Mater 2017;136:181–9.
[7] Nandam SH, Schwaiger R, Kobler A, Kübel C, Wang C, Ivanisenko Y, et al. Controlling shear band instability by nanoscale heterogeneities in metallic nanoglasses. J Mater Res 2021;36:2903–14.
[8] Wang C, Mu X, Chellali MR, Kilmametov A, Ivanisenko Y, Gleiter H, et al. Tuning the Curie temperature of $Fe_{90}Sc_{10}$ nanoglasses by varying the volume fraction and the composition of the interfaces. Scr Mater 2019;159:109–12.
[9] Adibi S, Branicio PS, Zhang Y, Joshi SP. Composition and grain size effects on the structural and mechanical properties of CuZr nanoglasses. J Appl Phys 2014;116:043522.
[10] Jing J, Krämer A, Birringer R, Gleiter H, Gonser U. Modified atomic structure in a Pd-Fe-Si nanoglass: a Mössbauer study. J Non-Cryst Solids 1989;113:167–70.
[11] Wang MM, Kiani MT, Parakh A, Jiang Y, Gu XW. Effect of grain size on iron-boride nanoglasses. J Mater Sci Technol 2023;141:116–23.
[12] Alexander AM, Hargreaves JSJ. Alternative catalytic materials: carbides, nitrides, phosphides and amorphous boron alloys. Chem Soc Rev 2010;39:4388–401.
[13] Pei Y, Zhou G, Luan N, Zong B, Qiao M, Tao F. Synthesis and catalysis of chemically reduced metal-metalloid amorphous alloys. Chem Soc Rev 2012;41:8140–62.
[14] Zhao M, Abe K, Yamaura SI, Yamamoto Y, Asao N. Fabrication of Pd-Ni-P metallic glass nanoparticles and their application as highly durable catalysts in methanol electro-oxidation. Chem Mater 2014;26:1056–61.
[15] Jiang Q, Lu H. Size dependent interface energy and its applications. Surf Sci Rep 2008;63:427–64.
[16] Shrestha S, Wang B, Dutta P. Nanoparticle processing: understanding and controlling aggregation. Adv Colloid Interface Sci 2020;279:102162.
[17] Shen J, Li Z, Yan Q, Chen Y. Reactions of bivalent metal ions with borohydride in aqueous solution for the preparation of ultrafine amorphous alloy particle. ChemInform 1993;97:8504–11.
[18] Wells S, Charles SW, Mørup S, Linderoth S, Wonterghem J van, Larsen J, et al. A study of Fe-B and Fe-Co-B alloy particles produced by reduction with borohydride. J Phys Condens Matter 1999;1:8199–208.
[19] Wang Y, Ai X, Cao Y, Yang H. Exceptional electrochemical activities of amorphous Fe-B and Co-B alloy powders used as high capacity anode materials. Electrochem Commun 2004;6:780–4.
[20] Wonterghem J van, Mørup S, Koch CJW, Charles SW, Wells S. Formation of ultrafine amorphous alloy particles by reduction in aqueous solution. Nature 1986;322:622–3.
[21] Yang Y, Li L, Chen G, Liu E. Synthesis and characterization of iron-based alloy nanoparticles for magnetorheological fluids. J Magn Magn Mater 2008;320:2030–8.
[22] Shao J, Xiao X, Fan X, Chen L, Zhu H, Yu S, et al. A low temperature mechanochemical synthesis and characterization of amorphous Ni-B ultrafine nanoparticles. Mater Lett 2013;109:203–6.
[23] Baláž P, Achimovičová M, Baláž M, Billik P, Cherkezova-Zheleva Z, Criado JM, et al. Hallmarks of mechanochemistry: from nanoparticles to technology. Chem Soc Rev 2013;42:7571–637.
[24] Avvakumov E, Senna M, Kosova N. Soft mechanochemical synthesis: a basis for new chemical technologies. first ed. New York: Kluwer Academic Publishers; 2001.
[25] Wu N, Su L, Yuan M, Wu J, Li Z. Nano-sized amorphous Cu-Zr alloy particles prepared by mechanochemical reaction. Mater Sci Eng 1998;257:357–60.
[26] Yang X, Yang B, Li X, Cao Y, Yu R. Structural-controlled chemical synthesis of nanosized amorphous Fe particles and their improved performances. J Alloys Compd 2015;651:551–6.
[27] Okumura H, Ishihara KN, Shingu PH, Park HS, Nasu S. Mechanical alloying of Fe-B alloys. J Mater Sci 1992;27:153–60.
[28] Calka A, Radlinski AP. Formation of amorphous FeB alloys by mechanical alloying. Appl Phys Lett 1991;58:119–21.